nature chemistry

SUPPLEMENTARY INFORMATION

DOI: 10.1038/NCHEM.1192

Large-Scale Screening of Hypothetical Metal-Organic Frameworks

Christopher E. Wilmer,[1] Michael Leaf,[1] Chang Yeon Lee,[2] Omar K. Farha,[2] Brad G. Hauser,[2] Joseph T. Hupp[2] and Randall Q. Snurr[1,*]

[1]Department of Chemical and Biological Engineering
Northwestern University, 2145 Sheridan Road, Evanston, IL 60208, USA

[2]Department of Chemistry, Northwestern University, 2145 Sheridan Road, Evanston, Illinois 60208, USA

* To whom correspondence should be addressed. E-mail: snurr@northwestern.edu

Table of contents

S1. Estimating the Number of Hypothetical Metal-Organic Frameworks

Here we provide some estimates on the number of possible hypothetical metal-organic frameworks (MOFs) given a library of modular building blocks of finite size (from here on assumed to be 100) and applying several simplifying assumptions.

First, consider the case of MOFs composed of only one type of inorganic building block and one type of organic building block. Let L be the number of organic building blocks (L as in "linkers") and C be the number of inorganic building blocks to choose from (C as in "corners"). Linkers may only connect with corners, and vice versa. The number of possible MOFs, N, is simply $N = L \times C$, which corresponds, for example, to 900 for L=90 and C=10.

Now consider the case where a unit-cell of a MOF contains M linkers (not to be confused with L: the number of linker types), which can be either of two types: A or B. Here the diversity of possible structures spans two dimensions: the ratio of A-linkers to B-linkers, and the number of possible arrangements of A and B linkers at a fixed ratio (see Figure S1).

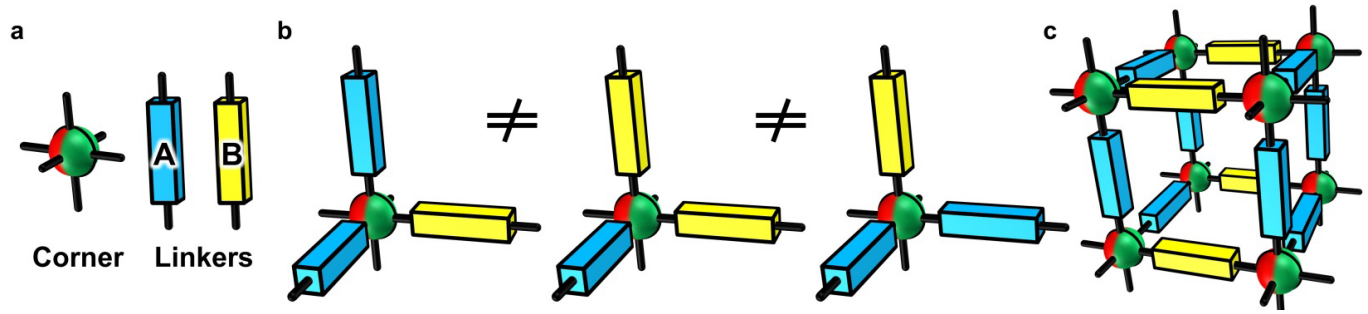

Figure S1. MOFs that contain two distinct linkers (A-type, *blue*, and B-type, *yellow*) **(a)** may vary in the ratio of A to B linkers **(b – left vs. middle)** or in the arrangement of those linkers at a fixed ratio **(b – left vs. right)**. A larger fragment of the schematic MOF framework is shown in **(c)** for clarity.

We can estimate a lower bound on the number of unique crystals by the number of ratios of component *types* (i.e., a unit-cell with two A-linkers and one B-linker cannot be the same crystal as one with one A-linker and 2 B-linkers). Calculating this lower bound is equivalent to finding the number of unordered sets of M balls of L colors (the answer is: $M + L - 1$ choose $L - 1$). However, two crystals, both with two A-linkers and one B-linker but in different positions, can either be physically identical (i.e., related by a symmetry operation) or unique (for example, if the corner is asymmetrical as in Figure S1). Thus, we can set an upper bound on the number of possible crystals by forming strings such as "BBA", "BAA", "BAB" and so forth. Thus, with a meager library of one corner and two linkers, the number, N, of possible MOFs is

$$\binom{M+L-1}{L-1} = \binom{3+2-1}{2-1} < N < 2^3 = L^M$$
$$4 < N < 8 \qquad \text{Eq. S1}$$

If we allow for more corners and linkers in our library (for example, C = 10, L = 90) but keep the constraint that MOFs may only use two linkers *simultaneously,* then we arrive at the modified expression,

$$\mathrm{C} \times \mathrm{L} \times \left[\left(\frac{\mathrm{L}-1}{2}\right)\binom{3+2-1}{2-1} - \mathrm{L} + 2\right] < N < C \times L \times \left[\left(\frac{\mathrm{L}-1}{2}\right)2^3 - \mathrm{L} + 2\right] \qquad \text{Eq. S2}$$

$$81{,}000 < N < 241{,}200$$

Finally, when we consider that linkers are themselves made from modular organic components, the number of hypothetical MOFs increases considerably. Let us define a linker as a combination of a backbone (e.g., benzene-1,4-dicarboxylic acid) and a functional group (e.g., methyl). Let B and F represent the number of backbones and functional groups in our library, respectively. In general, a single choice of backbone and functional group may result in many possible linkers, due to the number of ways the functional group may be arranged on the backbone (e.g., meta-, para-, and ortho-xylene) or simply due to the total number of functional groups (e.g., toluene vs. xylene). If we estimate, conservatively, that every backbone has only two possible arrangements for any given choice of functional group, then the number of linkers, L, is given by,

$$L = B \times F \times 2 \qquad \text{Eq. S3}$$

Substituting Eq. S3 into Eq. S2, assuming a library of 10 corners, 10 functional groups, and 80 backbones (100 building blocks total), corresponds to a lower bound of 25,600,000 and an upper bound of 89,560,000. Note that we have assumed all building blocks in this library are chemically compatible so that every piece is interchangeable (a reasonable assumption for an appropriately chosen chemical library).

In our generation procedure, we have used a library of 5 corners, 42 backbones, and 13 functional groups, although they are not all chemically, nor geometrically, compatible. If it were the case that from our library all corners could combine with all linkers (and all backbones with all functional groups, clearly not possible with building block **10** in Figure S2), we would expect between ~5.9 and ~20.9 million entries in our database rather than ~137 thousand.

S2. List of Modular Building Blocks

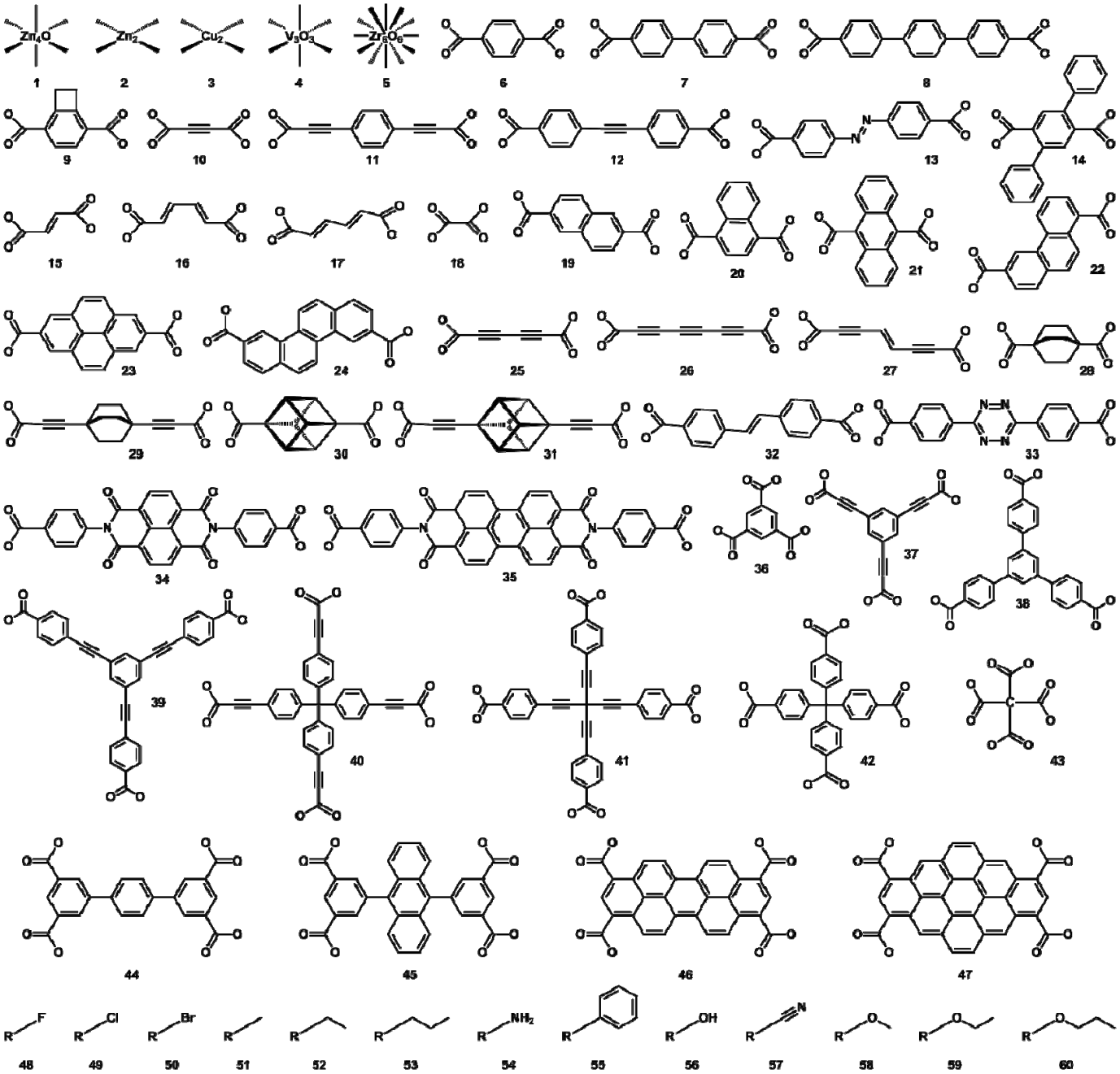

Figure S2. Full list of building blocks used to generate database of ~137,000 hypothetical MOFs. **1-5** are inorganic building blocks, **6-47** are organic building blocks and **48-60** are the functional groups. Building blocks 6 through 47 may be terminated with nitrogen atoms instead of carboxylic acid groups, yielding 102 building blocks in total.

The building blocks we used are shown in concise form in Figure S2. The inorganic building blocks **2** and **3** (referred to sometimes as paddlewheels) are able to coordinate to nitrogen containing compounds (e.g.,

pyrazine). Not shown then, in Figure S2 are all of the analogous building blocks terminated by nitrogen atoms instead of carboxylic acid groups.

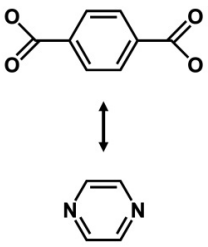

Figure S3. Building blocks in Figure S2 are shown with terminal carboxylate groups; however, every such building block also exists with a nitrogen terminated group, as well, for coordinating to paddlewheels.

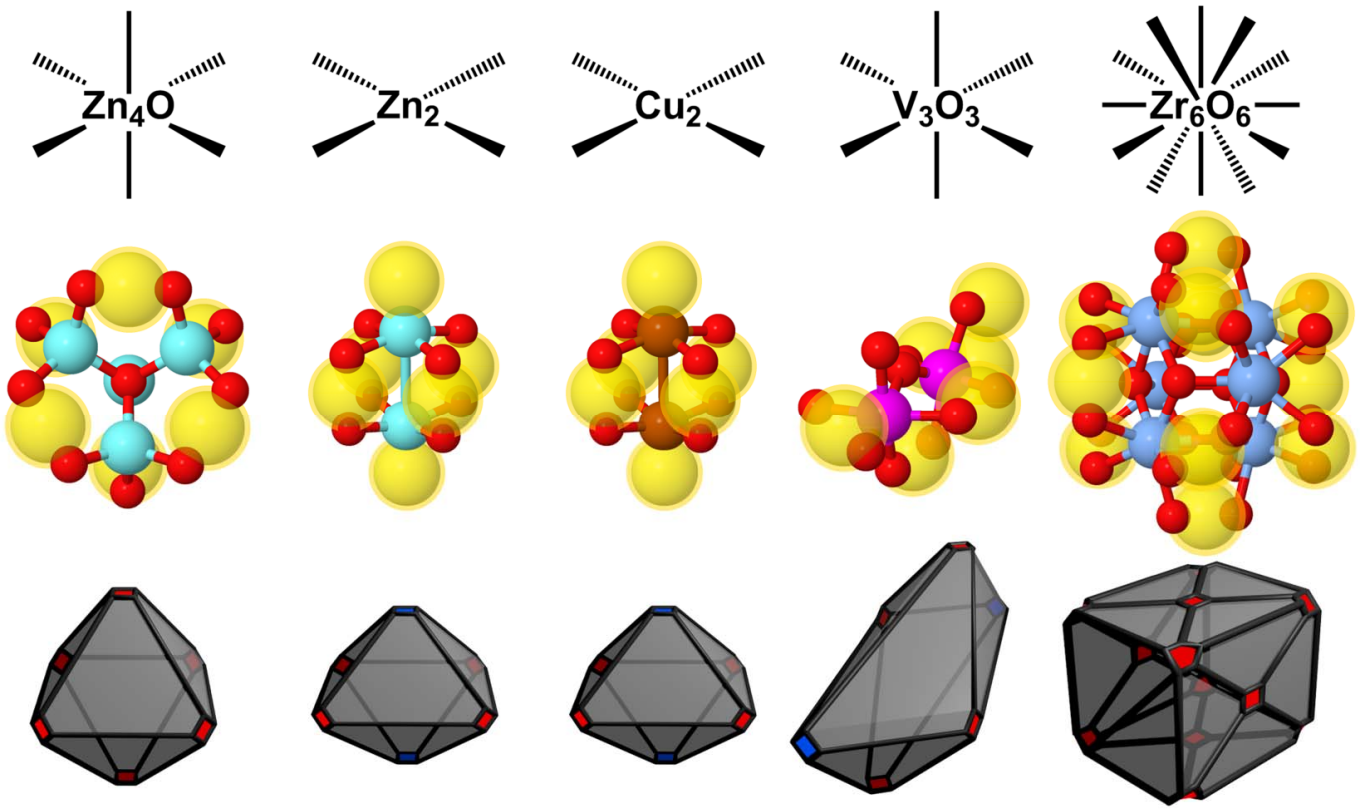

Figure S4. 3D structures of the metal containing building blocks organized into columns. Top row shows 2D schematic. Middle row shows 3D atomistic structure used with connection points indicated by translucent yellow spheres. The bottom row shows the representative geometry of the metal cluster, with colored patches indicated connection sites (red and blue patches are used to distinguish between connection sites with different chemistries required for bonding).

S3. Crystal Generator Algorithm

Building block details. In order to recombine building blocks into crystals, additional topological and geometrical information is manually assigned to each building block (see Figure S5). The topological information takes the form of numbered connection sites so that the generation algorithm can interpret instructions such as "connect building block **2,** site **3,** to building block **10,** site **1**". Additionally, this information is used as part of the algorithm's termination criteria; only when every connection site has been connected is a single MOF generation complete. The geometrical information takes the form of three "pseudo-atoms" and a list of angles for every connection site in the building block. The pseudo-atoms each possess a coordinate in 3d space, as well as a label (here referred to arbitrarily as *R*, *G*, or *B*). The purpose of the pseudo-atoms is to unambiguously specify the relative orientation of two connected building blocks. Specifically, given two connection sites *X* and *Y* and their corresponding pseudo-atoms R_X, G_X, B_X, and R_Y, G_Y, B_Y, the building blocks are oriented correctly when the coordinates of R_X equal R_Y, the coordinates of G_X equal G_Y, and the vector R_XB_X is anti-parallel to the vector R_YB_Y. Finally, if there are multiple "correct" orientations (for example, phenyl rings in a linear chain experience multiple energy minima of equal depth as a function of their relative orientations along the chain axis), the list of angles specifies alternate orientations, equivalent to rotating the pseudo-atoms about the *RB* axis by the specified angle.

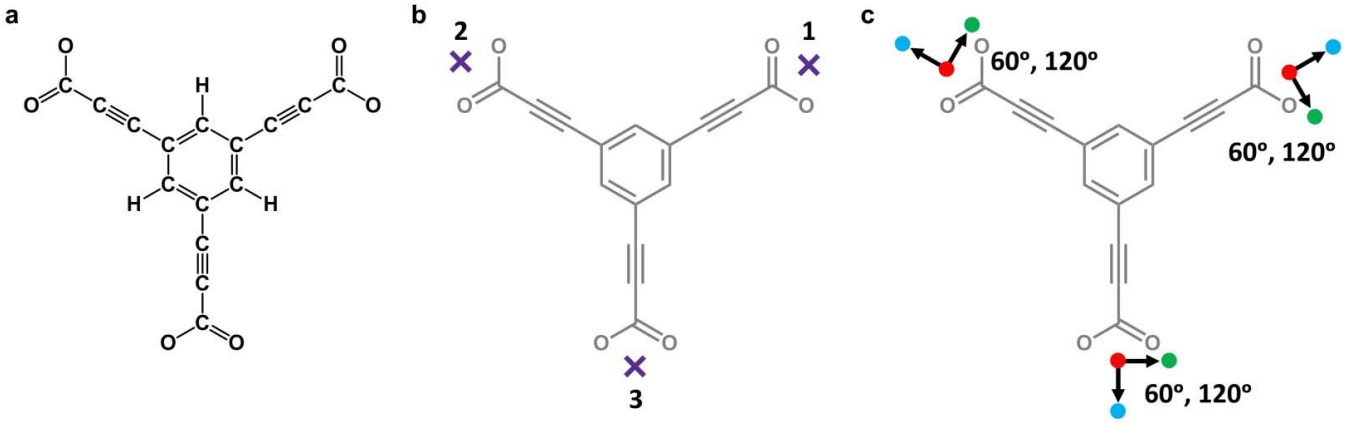

Figure S5. Encoded in the building blocks is the **(a)** atom composition and geometry, **(b)** topological information via numbered connection sites and **(c)** geometrical information via pseudo-atoms (colored as red, green and blue dots for *R*, *G* and *B* pseudo-atoms respectively) and lists of angles for alternative orientations.

Generation algorithm. The algorithm enumerates all possible combinations of building blocks in all possible arrangements. This is possible because the building blocks are numbered, and also because all possible arrangements of building blocks can be written as enumerable strings. For example, the string "1,2-3-1-2-3" means:

- "**1**, 2-3-1-2-3" → place a building block of type 1 anywhere
- "1, **2**-3-1-2-3" → select a building block of type 2 (not yet placed anywhere)

- "1, 2-**3**-1-2-3" → select its connection site 3
- "1, 2-3-**1**-2-3" → connect the selected building block to the 1st building block placed
- "1, 2-3-1-**2**-3" → connect the selected connection site to the 2nd connection site on the 1st building block
- "1, 2-3-1-2-**3**" → rotate the selected building block using the 3rd angle listed at the selected connection site

This arrangement leads to a nonsensical connection of two inorganic building blocks, and so the generator would skip to the next arrangement, namely, "1, 2-3-1-2-4", and so-forth. The generation procedure is summarized in Figure S6. In this example, if "1,2-3-1-2-3" was the n^{th} arrangement, then "1,2-3-1-2-4" would be called the $(n+1)^{th}$ arrangement. The number of all possible arrangements for a set of a building blocks is n_{max}. In our screening procedure, if no logical MOF structure could be generated in the first 64,000 arrangements of the chosen building blocks, then the arrangement string was incremented by a large random value (e.g., "1,2-3-1-2-4" might jump to "4,1-3-2-4-4"). If no MOF structure could be found after 5 such increments, then the next set of building blocks was chosen (see Figure S6).

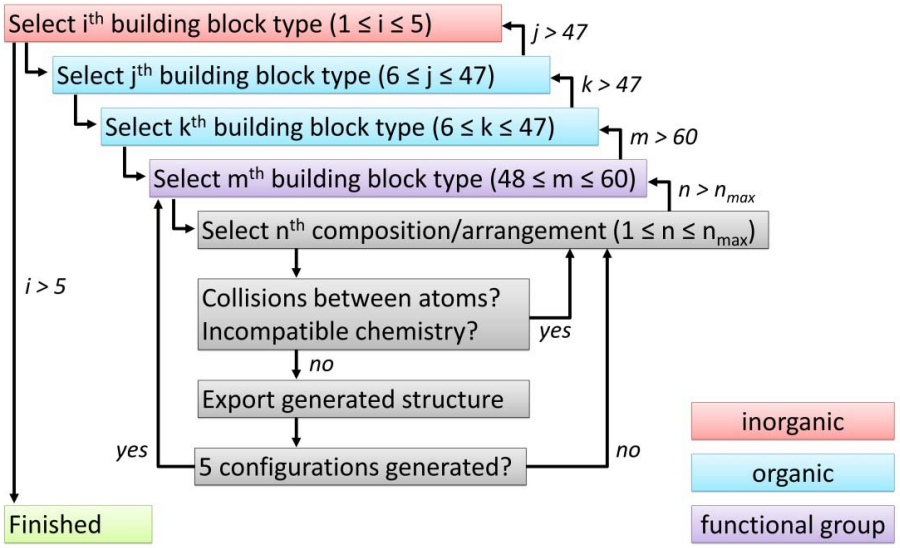

Figure S6. A flowchart depicting how hypothetical MOFs are enumeratively generated from a library of building blocks. The upper and lower limits of *i*, *j*, *k*, and *m* refer to the numbered building blocks in Figure S2. In the "select n^{th} composition/arrangement" step, the total number and arrangement of building blocks is encoded in an enumerable string. In the particular library of building blocks we used, functional groups could be connected in any location where a hydrogen atom is otherwise bonded to a carbon atom, provided no atomic collisions occur. In the following "collisions between atoms" step, structures were "colliding" if any two atoms were closer than one angstrom apart. This distance was used so as not to discard potentially interesting MOFs due slight structural errors introduced in the generation process.

S4. Generated Structure Validation

Comparing experimental and generated structures. We investigated the generated structures by comparing the coordinates of their atoms against the coordinates of the atoms in the experimental and energetically optimized structures. However, if the unit cell dimensions of two structures differed even only slightly, then the distance between corresponding atoms in either structure will eventually diverge. For this reason we chose to make pairwise comparisons of fragments of crystals that shared one atom (chosen arbitrarily) identically at the origin. These fragments were superimposed using the feature by the same name in Materials Studio. Fragments were defined by selecting a metal atom center and all atoms that could be reached from the metal atom by traversing 7 bonds (an alternative approach would have been to include atoms within a specified radius of a chosen atom center, but this does not guarantee that each fragment has the same total number of atoms). The program orients and translates one fragment relative to the other such that the interatomic distances between the atoms of both fragments are minimized. The degree to which one fragment matches the other is measured by the average root-mean-squared distance over all pairs of nearest atoms. Hydrogen atoms were ignored as they are often missing from crystallographic data. Average differences in atomic positions were less than ~0.1 Å except in the case of the optimized PCN-14, although even in this case the methane adsorption isotherm was not greatly affected (see Figure 2 in the main text).

Table S1. Comparisons of generated vs. empirical structures by matching interatomic distances. Table shows average root-mean-squared distance between matched atoms.

	Experimental vs. Pseudo	Experimental vs. Pseudo-Optimized	Fragment Size (# of atoms)
HKUST-1	< 0.001 Å	0.004 Å	74
IRMOF-1	0.013 Å	0.032 Å	77
PCN-14	0.113 Å	0.696 Å	74
MIL-47	0.028 Å	0.089 Å	131

Energetic structure relaxations. These geometry optimizations were performed with the Forcite module of Materials Studio using an algorithm which is a cascade of the steepest descent, adjusted basis set Newton-Raphson, and quasi-Newton methods. The bonded and the short range (van der Waals) non-bonded interactions between the atoms were modeled using the Universal Force Field (UFF).[1] In this force field, bond stretching is described by a harmonic term, angle bending by a three-term Fourier cosine expansion, torsions and inversions by cosine-Fourier expansion terms, and the van der Waals interactions by the Lennard-Jones potential.

S5. Database of Hypothetical Metal-Organic Frameworks – Available Online

The full database of hypothetical crystals is available online at hmofs.northwestern.edu. Every crystal structure may be downloaded in the CIF format. Pore-size distributions and powder x-ray diffraction spectra may be downloaded in the comma separated value (CSV) format (despite the format name, data is separated using white space characters). The reader is encouraged to unearth structure-property relationships we have not recognized in the main text (of which there are certainly many, for example, see Figure S7).

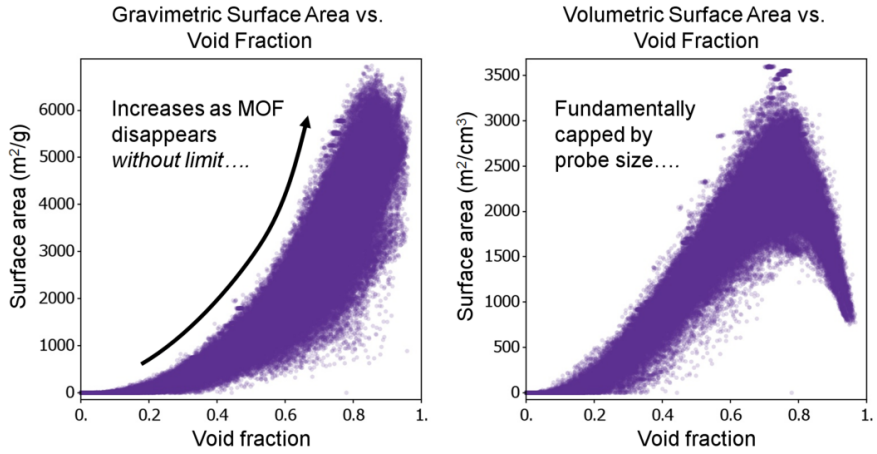

Figure S7. Two structure-property relationships found in our database that are purely geometric in nature. Importantly, this data suggests that volumetric surface area is fundamentally capped to a value determined by the probe size used, whereas gravimetric surface area shows no obvious limit.

S6. Computing Methane Adsorption

Atomistic grand canonical Monte Carlo (GCMC) simulations were performed to estimate the adsorption isotherms of CH_4 in all of the hypothetical MOFs. Interaction energies between non-bonded atoms were computed through the Lennard-Jones (LJ) potential:

$$V_{ij} = 4\varepsilon_{ij}\left[\left(\frac{\sigma_{ij}}{r_{ij}}\right)^{12} - \left(\frac{\sigma_{ij}}{r_{ij}}\right)^{6}\right]$$

where i and j are interacting atoms, and r_{ij} is the distance between atoms i and j. ε_{ij} and σ_{ij} are the LJ well depth and diameter, respectively. LJ parameters between atoms of different types were calculated using the Lorentz-Berthelot mixing rules (i.e., geometric average of well depths and arithmetic average of diameters). LJ parameters for framework atoms were taken from the Universal Force Field (UFF).[1] The methane molecules were modeled using the TraPPE[2] force field, which was originally fit to reproduce the vapor-liquid coexistence curve of methane. In this force field, methane is modeled as a single sphere (parameters shown in Table S1). Whereas in prior work, framework parameters were taken from DREIDING[3] and only from UFF when a

parameter did not exist in DREIDING, here we used only parameters from UFF. We examined the effect of this choice by comparing methane simulations using both parameter sets (DREIDING + UFF vs. UFF only) on six MOFs that are diverse in chemical composition and geometry (see Figure S8).

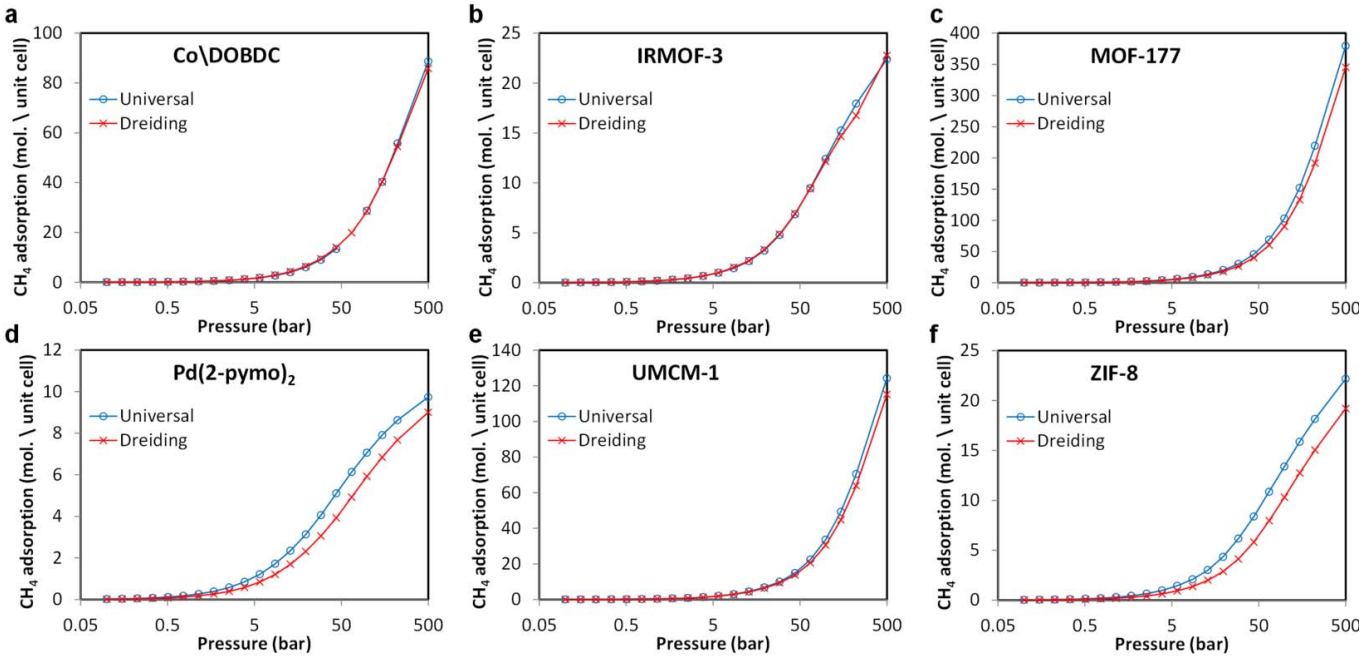

Figure S8. A comparison of absolute methane adsorption isotherms at 298 K for six diverse MOFs, using two different sets of force field parameters (**red** – DREIDING on all framework atoms when availabled, otherwise UFF, **blue** – UFF only). MOF structures used: Co\DOBDC,[4] IRMOF-3,[5] MOF-177,[6] Pd(2-pymo)$_2$,[7] UMCM-1,[8] and ZIF-8.[9] Agreement was generally good, with UFF predicting higher adsorption capacity on average. For the purpose of large-scale screening, the UFF parameters are likely sufficient.

Table S2. LJ parameters for methane and framework atoms in all hypothetical MOFs.

Atom type	σ (Å)	ε/k_B (K)
C	3.43	52.83
O	3.12	30.19
H	2.57	22.14
N	3.26	34.72
F	2.997	25.16
Cl	3.517	114.23
Br	3.73	126.30
Zn	2.46	62.40
Cu	3.114	2.516
V	2.80	8.05
Zr	2.783	34.72
CH_4	3.75	148.0

All GCMC simulations of methane adsorption included an *M*-cycle equilibration period followed by an *M*-cycle production run, where *M* was 500, 2500, or 12,500 as described in the main text (see Figure 4). A cycle consists of *n* Monte Carlo steps; where *n* is equal to the number of molecules (which fluctuates during

a GCMC simulation). All simulations included random insertion, deletion, and translation moves of molecules with equal probabilities. Atoms in the MOF were held fixed at their crystallographic positions. An LJ cutoff distance of 12.8 Å was used for all simulations. A 2x2x2 unit cell of every crystal was used for the simulations. Methane adsorption was simulated at a single pressure, 35 bar, at 298 K for all crystals. In addition, a complete isotherm was calculated (over a wide range of pressures) for the four MOFs (HKUST-1, IRMOF-1, PCN-14, and MIL-47) described in Figure 2 of the main text. Fugacities needed to run the GCMC simulations were calculated using the Peng-Robinson equation of state. GCMC simulations report the absolute adsorption data, which are then used to compute the excess adsorption data for comparison with experimental data using the relation,

$$N_{total} = N_{excess} + \rho_{gas} \times V_p$$

where ρ_{gas} is the bulk density of the gas at simulation conditions, calculated with the Peng-Robinson equation of state, and V_p is the pore volume calculated by the helium insertion method as detailed elsewhere.[10]

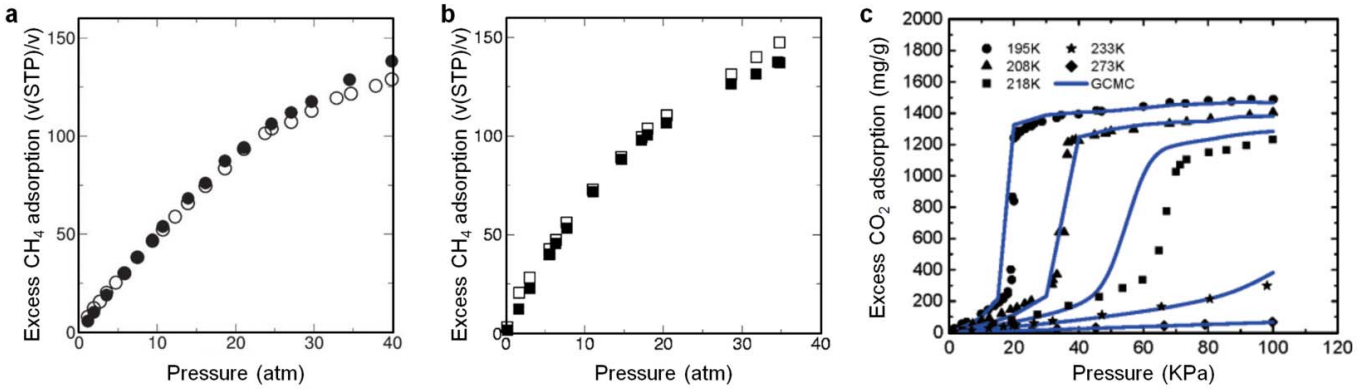

Figure S9. Comparison between experimental and simulated adsorption isotherms of CH_4 at 298 K for **(a)** IRMOF-1 and **(b)** IRMOF-6 (open symbols, experimental results; closed symbols, simulation results) using the same simulation methodology as in this article. Reproduced with permission from Ref. [11]. Copyright 2004, American Chemical Society. **c,** Comparison between experimental and simulated adsorption of CO_2 in IRMOF-1 at several temperatures. Reproduced with permission from Ref. [12]. Copyright 2008, American Chemical Society.

MOF-#1 from main text. The structure labeled "MOF-#1" in Figure 4f of the main text is composed of building blocks **3**, **31** (nitrogen terminated), **35**, and **52** as depicted in Figure S2. The CIF structure is available in the online database along with all others.

Lower temperature (290 K) PCN-14 simulated methane adsorption isotherm. The methane adsorption isotherm was simulated for the PCN-14 structure identically to the above method, but at 290 K to better represent the experiment conducted by Ma *et al*.[13] A BET surface area was calculated[14] over a pressure range of $0.003 < P/P_0 < 0.1$ from a simulated N_2 isotherm at 77 K (see Figure S10, right) using the same parameters as above and 5000 cycles per data point.

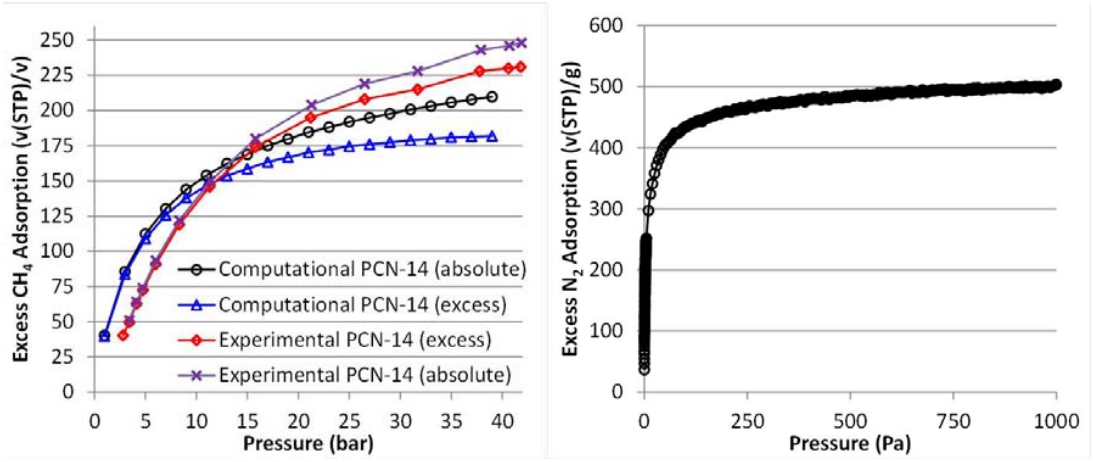

Figure S10. (***left***) Simulated and experimental methane adsorption isotherms for PCN-14 at 290 K. Experimental data from Ma *et al*.[13] (***right***) Simulated N_2 isotherm at 77 K.

S7. Experiments: General Procedures, Materials, and Instrumentation

All air- or water-sensitive reactions were carried out under a dry nitrogen atmosphere using standard Schlenk techniques. Reagents and reagent-grade solvents were purchased from either VWR, Strem or Aldrich Chemical Company and used as received. Silica gel was purchased from Sorb. Tech. ^{1}H and ^{13}C NMR spectra were recorded on a Bruker 500 FT-NMR spectrometer (499.773 MHz for ^{1}H, 125.669 MHz for ^{13}C). ^{1}H NMR data are reported as follows: chemical shift (multiplicity (b = broad singlet, s = singlet, d = doublet, dd = doublet of doublets, ddd = doublet of doublets of doublets, t = triplet, q = quartet, and m = multiplet), integration, and peak assignments, coupling constants). ^{1}H and ^{13}C chemical shifts are reported in ppm from TMS with residual solvent resonances as internal standards. Powder X-ray diffraction (PXRD) data were recorded on a Rigaku ATX-G diffractometer using nickel-filtered Cu Kα radiation. Data were collected over the range of $5^\circ < 2(\theta) < 40^\circ$ in 0.05° steps at a scan rate of 2°/min. Supercritical CO_2 processing was performed with a Tousimis™ Samdri® PVT-30 critical point dryer. All manipulations of activated samples were done in an argon atmosphere glove box to avoid contact with water. Surface area calculations used nitrogen adsorption isotherms measured at 77.3 K on a Tristar 3020 by Micromeritics. The BET surface area was calculated between $0.003 < P/P_0 < 0.1$ and the correlation was 0.99993 and the intercept positive. An activated sample (28 mg) was placed into a preweighed glass holder. Analysis temperature was held at a constant 77.3 K in a liquid nitrogen bath. High-

pressure (1 to 35 bar) methane adsorption measurements were carried out on an HPVA-100 from VTI Instruments. The sample was held at 298 K in a circulating water bath. A 2 cc stainless steel sample holder was loaded with the activated sample (258 mg) in an argon atmosphere glove box and sealed prior to analysis. All gases (He, N_2, and CH_4) used for analysis were of ultra-high purity grade (>99.99% pure) from Airgas and were used without further purification. Microwave heating was carried out using an automatic single-mode synthesizer (Initiator^{TM} 2.0) from Biotage, which produces a radiation frequency of 2.45 GHz.

S8. Experiments: Synthesis of Ligand Precursors, Ligand, and NOTT-107

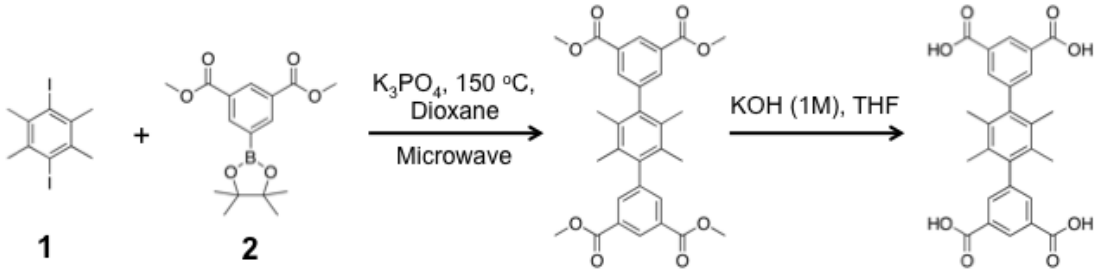

Figure S11. Synthesis of tetracarboxylate ligand **4**.

Synthesis of 3. 1,4-Diiodo-2,3,5,6-tetramethylbenzene (**1,** purchased from VWR) (0.60 g, 1.55 mmol), 3,5-Bis(methoxycarbonyl) phenylboronic acid pinacol ester (**2,** prepared following Chen et al.[15]) (1.09 g, 3.41 mmol), K_3PO_4 (1.97 g, 9.30 mmol) and dioxane (15 ml) were combined in 10-20 ml capacity microwave vials and degassed for 10 min with nitrogen. $Pd(PPh_3)_4$ (0.040 g, 0.03 mmol) was added and the vial was microwave heated with stirring at 150 ^oC for 6 h. After cooling, CH_2Cl_2 (30 mL) was added and the organic layer was washed with water (20 mL × 3). The organic layer was dried over $MgSO_4$ and evaporated under vacuum. The resulting solid was washed with MeOH and then dried under vacuum to give a white solid (0.56 g, 70%). ^1H NMR (500 MHz, $CDCl_3$): δ 8.73 (t, *J* = 1.5Hz 2H), 8.10 (d, J = 1.6Hz, 4H), 3.99 (s, 12H), 1.94 (s, 12H); ^{13}C NMR (125MHz, $CDCl_3$) δ 166.4, 143.4, 139.8, 134.8, 132.0, 130.9, 129.1, 52.5, 18.2.

Synthesis of 4. To a stirring solution of **3** (1 g, 1.93 mmol) in THF (50 mL), KOH (120 mL of a 1 M aqueous solution, 120 mmol) was added. The mixture was refluxed for 15 h until it became clear. THF was removed using a rotary evaporator and the remaining aqueous solution was acidified to pH 2 using concentrated HCl (15 mL of a 37% aqueous solution). The resulting precipitate was collected via filtration, washed with H_2O (200 mL), and dried under high vacuum to afford **4** as a white solid (0.80 g 90%). ^1H NMR (500 MHz, DMSO-*d*6): δ 8.51 (s, 2H), 7.91 (s, 4H), 1.88 (s, 12H); ^{13}C NMR (125Mz, $CDCl_3$) δ 166.5, 142.6, 139.3, 133.9, 131.7, 131.4, 128.4, 17.9.

Synthesis of NOTT-107. We were unaware at the time of synthesis that the NOTT-107 structure had been reported previously by Lin *et al*.,[16] and consequently our experimental procedure is different. A mixture of $Cu(NO_3)_2.2.5H_2O$ (600 mg, 2.6 mmol) and **4** (360 mg, 0.78 mmol) was dissolved in a mixture of DMF (60 mL) in a beaker. Then 60 ml of ethanol and 24 drops of conc. HCl were added to the solution and mixed well. This solution was divided between 15 6-dram vials. The vials were capped and placed into an oven at 80 °C for 24 h. The resulting teal crystalline powder was combined and washed with DMF.

Activation of NOTT-107. Prior to drying, DMF/EtOH-solvated MOF samples were soaked in absolute ethanol, replacing the soaking solution every 24 h for 3 days. After soaking, the ethanol-containing samples were placed inside the supercritical CO_2 dryer and the ethanol was exchanged with CO_2(liq.) over a period of 8 h. During this time the liquid CO_2 was vented under positive pressure for three minutes every two hours. The rate of venting of CO_2(liq.) was always kept below the rate of filling so as to maintain a full drying chamber. Then the chamber was sealed and the temperature was raised to 38 ºC (i.e., above the critical temperature for carbon dioxide), at which time the chamber was slowly vented over the course of 15 h. The color of the MOF changed from teal to dark blue. The collected MOF sample was then stored inside an inert-atmosphere glovebox until further analysis.

Prior to sorption measurements, the sample was evacuated at room temperature for three hours, then brought to 110 °C over four hours.

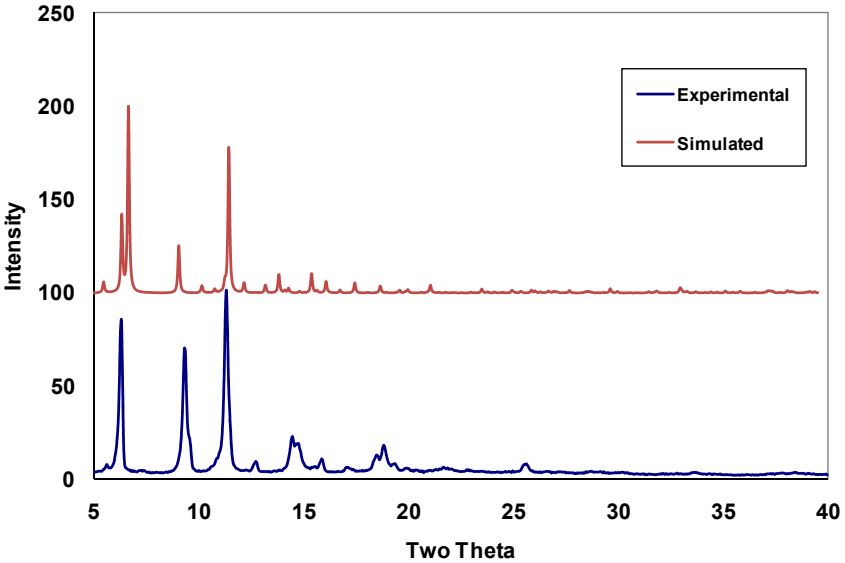

Figure S12. PXRD pattern of NOTT-107.

References

1. Rappé, A. K., Casewit, C. J., Colwell, K. S., Goddard III, W. A. & Skiff, W. M. UFF, a full periodic table force field for molecular mechanics and molecular dynamics simulations. *J. Am. Chem. Soc.* **114**, 10024-10035 (1992).
2. Martin, M. G. & Siepmann, J. I. Transferable potentials for phase equilibria. 1. United-atom description of n-alkanes. *J. Phys. Chem. B* **102**, 2569–2577 (1998).
3. Mayo, S. L., Olafson, B. D. & Goddard III, W. A. DREIDING: a generic force field for molecular simulations. *J. Phys. Chem* **94**, 8897-8909 (1990).
4. Dietzel, P. D. C., Morita, Y., Blom, R. & Fjellvåg, H. An in situ high-temperature single-crystal investigation of a dehydrated metal-organic framework compound and field-induced magnetization of one-dimensional metal-oxygen chains. *Angew. Chem. Int. Ed.* **44**, 6354-6358 (2005).
5. Eddaoudi, M. *et al.* Systematic design of pore size and functionality in isoreticular MOFs and their application in methane storage. *Science* **295**, 469-472 (2002).
6. Chae, H. K. *et al.* A route to high surface area, porosity and inclusion of large molecules in crystals. *Nature* **427**, 523-527 (2004).
7. Navarro, J. A. R. *et al.* H_2, N_2, CO, and CO_2 sorption properties of a series of robust sodalite-type microporous coordination polymers. *Inorganic Chemistry* **45**, 2397-2399 (2006).
8. Koh, K., Wong-Foy, A. G. & Matzger, A. J. A crystalline mesoporous coordination copolymer with high microporosity. *Angew. Chem. Int. Ed.* **47**, 677-680 (2008).
9. Park, K. S. *et al.* Exceptional chemical and thermal stability of zeolitic imidazolate frameworks. *Proc. Natl. Acad. Sci. U.S.A.* **103**, 10186-10191 (2006).
10. Frost, H., Düren, T. & Snurr, R. Q. Effects of surface area, free volume, and heat of adsorption on hydrogen uptake in metal-organic frameworks. *J. Phys. Chem. B* **110**, 9565-9570 (2006).
11. Düren, T., Sarkisov, L., Yaghi, O. M. & Snurr, R. Q. Design of new materials for methane storage. *Langmuir* **20**, 2683-2689 (2004).
12. Walton, K. S. *et al.* Understanding inflections and steps in carbon dioxide adsorption isotherms in metal-organic frameworks. *J. Am. Chem. Soc.* **130**, 406-407 (2008).
13. Ma, S. *et al.* Metal-organic framework from an anthracene derivative containing nanoscopic cages exhibiting high methane uptake. *J. Am. Chem. Soc.* **130**, 1012–1016 (2008).
14. Walton, K. S. & Snurr, R. Q. Applicability of the BET method for determining surface areas of microporous metal−organic frameworks. *J. Am. Chem. Soc.* **129**, 8552-8556 (2007).
15. Chen, Z. X. *et al.* A new multidentate hexacarboxylic acid for the construction of porous metal-organic frameworks of diverse structures and porosities. *Cryst. Growth Des.* **10**, 2775-2779 (2010).
16. Lin, X. *et al.* High capacity hydrogen adsorption in Cu(II) tetracarboxylate framework materials: The role of pore size, ligand functionalization, and exposed metal sites. *J. Am. Chem. Soc.* **131**, 2159-2171 (2009).